Friction drag of a spherical particle in a liquid crystal above the isotropic-nematic transition

Jun-ichi Fukuda,[1,2,*] Holger Stark,[3] and Hiroshi Yokoyama[1,2]

[1]*Nanotechnology Research Institute, National Institute of Advanced Industrial Science and Technology (AIST), 1-1-1 Umezono, Tsukuba 305-8568, Japan*

[2]*Liquid Crystal Nano-System Project, ERATO/SORST, Japan Science and Technology Agency, 5-9-9 Tokodai, Tsukuba 300-2635, Japan*

[3]*Fachbereich Physik, Universität Konstanz, D-78457 Konstanz, Germany*

We study the friction drag of a spherical particle in the isotropic phase of a nematic liquid crystal close to the isotropic-nematic transition point. To describe the orientational order in the liquid crystal, the second-rank tensor order parameter $Q_{\alpha\beta}$ is employed. We solve the hydrodynamic equations for $Q_{\alpha\beta}$ and the fluid velocity v in order to determine the friction drag. In our discussion of the friction drag, we concentrate on four parameters: the temperature, the surface order parameter, the particle radius, and the Ericksen number Er (characterizing the ratio of the viscous force to the elastic force). The temperature dependence of the friction drag agrees well with experiments that show an increasing friction drag when the isotropic-nematic phase transition is approached from above. Furthermore the friction drag increases with the surface order parameter due to the more pronounced surface nematic layer, and for larger particles it is less affected by this layer. Finally, we observe that in the range of Er we study, the friction drag is almost independent of Er although flow-induced order occurs for sufficiently large Er and surface order parameter.

PACS number(s): 61.30.Dk, 47.50.+d, 82.70.Dd, 83.85.Pt

I. INTRODUCTION

Particles in a fluid have long been an important subject in hydrodynamics from the viewpoint of technological application as well as in a fundamental sense. Well-known properties of rigid spherical particles in a simple isotropic fluid include the Stokes law [1–3]; a particle moving with velocity v_0 experiences a drag force $f_S = 6\pi R_0 \eta v_0$ (here R_0 is the particle radius and η_0 is the shear viscosity of the fluid). The important Stokes-Einstein formula [1,2,4–6] relates the Brownian motion of a suspended particle with friction; the self-diffusion coefficient D of particles is given by $D = k_B T / 6\pi\eta R_0$, where k_B is the Boltzmann constant and T is the temperature. In his pioneering studies on colloidal dispersions, Einstein also showed that the effective shear viscosity η_{eff} of a dilute suspension of rigid spheres with volume fraction ϕ satisfies $\eta_{\text{eff}}/\eta = 1 + 5/2\phi$ [1,2,5]. Those findings about the hydrodynamic features of particles in an isotropic fluid constitute part of the basis of colloidal science.

More complicated but interesting behavior can be expected when the fluid surrounding the particles possesses internal degrees of freedom expressed by further hydrodynamic variables besides mass density (supposed to be constant in an incompressible fluid) and momentum density. One of the typical and well-known examples of such fluids is a liquid crystal [7,8], which shows a rich variety of mesophases depending on temperature and its molecular architecture. A nematic phase, characterized by long-range orientational order and the absence of positional order of the constituent molecules, is the simplest example of liquid crystal mesophases and has long been an important subject of liquid crystal science.

There have been several theoretical and numerical studies focusing on the hydrodynamics of a nematic liquid crystal in the presence of particles (spheres [9–16] or cylinders [17–19]). In the case of small particle velocity (to be precise, small Ericksen number characterizing the ratio of the viscous force to the elastic force), it has been shown that the friction coefficient depends on the direction of the particle motion with respect to the orientation of the background nematic liquid crystal [10,12–14,17,18]. When the particle velocity is large enough, strong distortions of the orientation profile and the resulting motion of the topological defect accompanying the particle have been suggested by numerical calculations [15,16,19]. Earlier experimental studies using a falling-ball apparatus [20,21], image processing of the Brownian motion [22], or Mössbauer technique [23,24] did not focus on the anisotropic nature of the particle diffusion (or the friction tensor) in a nematic liquid crystal. However, such an anisotropy has been identified experimentally using optical tweezers [25] or direct imaging of Brownian motion [26] in quantitative agreement with previous numerical studies [13,14].

In the present paper, we consider the effect of a liquid crystal above the isotropic-nematic (I-N) transition on the hydrodynamic properties of a suspended spherical particle. It has been argued since the pioneering theoretical work by Sheng [27] that a nematic phase can wet a surface even when the bulk is in an isotropic state. In our recent work [28], we have shown that a spherical particle is also wetted by a nematic phase, although due to curvature the properties of the surface layer are different from those on a flat substrate. It is therefore natural to expect that the nematic wetting layer at the surface of a particle should affect its hydrodynamic behavior, in particular its Brownian motion. Several experimental studies have been performed concerning the Brownian motion of particles suspended in an isotropic phase of a nematic liquid crystal [22,24,29]. How the particle diffusion near the transition point is influenced by temperature was

*Electronic address: fukuda.jun-ichi@aist.go.jp

intensively studied by Böttger *et al.* [29] using dynamic light scattering. They found that the effective hydrodynamic radius of a particle R_{eff}, deduced from the Stokes-Einstein relation, increases when the I-N transition is approached from above. They attributed it to the increase in the surface-nematic-layer thickness when the temperature decreases.

However, to our knowledge, there have been no theoretical or numerical studies to discuss the hydrodynamics of a liquid crystal above but close to the I-N transition in the presence of particles. The purpose of this paper is to present our numerical attempt to investigate the hydrodynamics of a liquid crystal around a particle when the liquid crystal is isotropic in the bulk and nematic order is induced at the particle surface due to rigid normal anchoring. We employ a second-rank tensor order parameter [7,30] for the description of the orientational order because we have to pay attention to both the strength and the direction of the orientational order of the liquid crystal. We consider the case where a spherical particle is fixed in a liquid crystal that flows with constant velocity at infinity. By solving the hydrodynamic equations for the orientational tensor order parameter and the fluid velocity, we determine the orientation and the velocity profiles around the particle, which enable us to calculate the friction drag of a spherical particle in a liquid crystal above the I-N transition. The important variables in the present problem other than material parameters are the strength of the surface order, the temperature, the particle radius, and the fluid velocity at infinity. We present our numerical results with a focus on the dependence of the friction force on those four variables.

Recent growing attention to liquid crystal colloid dispersions [31–38] has motivated several experimental studies to investigate how the I-N transition of the host liquid crystal influences the static and dynamic properties of liquid crystal colloidal dispersion [39,40]. Previous theoretical attempts concerning liquid crystal colloids close to the I-N transition have been restricted to the investigation of the static nature [28,41–45]. We believe that our present study will provide basic knowledge for further investigations of the dynamical aspects of liquid crystal colloids close to the I-N transition.

The organization of this article is as follows: Section II gives a detailed explanation about the set of hydrodynamic equations for the orientational order parameter and the fluid velocity, together with our numerical treatment. In Sec. III, we present the results of our numerical calculation. Section IV concludes this article.

II. MODEL

A. Free energy and the molecular field

We use a symmetric and traceless second-rank tensor $Q_{\alpha\beta}$ for the description of the orientational order of a liquid crystal. Since de Gennes proposed the use of a tensor order parameter for the discussion of the I-N phase transition [30], it has been extensively used to investigate various phenomena associated with the I-N transition theoretically. Following de Gennes, we can write the free energy density of a nematic liquid crystal in terms of $Q_{\alpha\beta}$ as

$$f\{Q_{\alpha\beta}\} = \frac{1}{2}A \, \text{Tr} \, \mathbf{Q}^2 - \frac{1}{3}B \, \text{Tr} \, \mathbf{Q}^3 + \frac{1}{4}C(\text{Tr} \, \mathbf{Q}^2)^2$$
$$+ \frac{1}{2}L_1 \partial_\gamma Q_{\alpha\beta} \partial_\gamma Q_{\alpha\beta}, \tag{1}$$

where A, B, C, and L_1 are phenomenological coefficients and hereafter we take summations over repeated greek indices denoting the Cartesian coordinates x, y, and z. Tr implies taking the trace of a tensor, i.e., $\text{Tr} \, \mathbf{Q}^2 = Q_{\alpha\beta}Q_{\beta\alpha}$ and $\text{Tr} \, \mathbf{Q}^3 = Q_{\alpha\beta}Q_{\beta\gamma}Q_{\gamma\alpha}$. The first three terms of Eq. (1) constitute the bulk energy in terms of a Landau-de Gennes expansion and the fourth term is the elastic energy. For simplicity we adopt the one-constant approximation for the elastic energy and do not take into account other terms allowed from symmetry ($L_2 \partial_\beta Q_{\alpha\beta} \partial_\gamma Q_{\alpha\gamma}$ and $L_3 \partial_\gamma Q_{\alpha\beta} \partial_\beta Q_{\alpha\gamma}$). The molecular field that appears in the hydrodynamic equations given below is defined by

$$H_{\alpha\beta} \equiv -\frac{\delta}{\delta Q_{\alpha\beta}} \int d\mathbf{r} \, f\{Q_{\alpha\beta}\}$$
$$= -AQ_{\alpha\beta} + BQ_{\alpha\gamma}Q_{\gamma\beta} - C(\text{Tr} \, \mathbf{Q}^2)Q_{\alpha\beta} + L_1\nabla^2 Q_{\alpha\beta}. \tag{2}$$

Since there are already many phenomenological parameters, we simplify the discussion by rescaling the order parameter as $Q_{\alpha\beta} = s\bar{Q}_{\alpha\beta}$ with $s = 2\sqrt{6}B/9C$. The molecular field in terms of $\bar{Q}_{\alpha\beta}$ reads

$$H_{\alpha\beta} = \frac{\Delta f}{s}\bar{H}_{\alpha\beta}$$
$$= \frac{\Delta f}{s}\left\{ -\tau\bar{Q}_{\alpha\beta} + \frac{3\sqrt{6}}{4}\bar{Q}_{\alpha\gamma}\bar{Q}_{\gamma\beta} \right.$$
$$\left. - (\text{Tr} \, \mathbf{Q}^2)\bar{Q}_{\alpha\beta} + \xi_R{}^2\nabla^2\bar{Q}_{\alpha\beta} \right\}. \tag{3}$$

Here $\tau \equiv A/Cs^2 = 27AC/8B^2$ is the reduced temperature. The unit of the free energy $\Delta f \equiv Cs^4 = 64B^4/729C^3$ is associated with the latent heat. We have also defined the characteristic length associated with the nematic coherence length

$$\xi_R \equiv \sqrt{\frac{L_1}{Cs^2}} = \sqrt{\frac{27L_1C}{8B^2}}. \tag{4}$$

We notice that in a strict sense the nematic coherence length at the transition point is $2\sqrt{2}\xi_R$, which is about 10 nm [28].

We here summarize the bulk transition properties. The first-order I-N transition is located at $\tau = 1/8 = 0.125$ and the nematic order parameter at the transition point is given by $\bar{Q}_{\alpha\beta} = \bar{Q}_0[n_\alpha n_\beta - (1/3)\delta_{\alpha\beta}]$ with $\bar{Q}_0 = \sqrt{6}/4 \simeq 0.612$ (here $\mathbf{n}$ is an arbitrary unit vector corresponding to the director). In this study we are interested in the cases where the bulk liquid crystal is in the isotropic state, therefore we always set $\tau \geqslant 1/8$ in the numerical calculations.

B. Hydrodynamic equations

There have been several theoretical attempts to formulate the set of hydrodynamic equations for the order parameter

$Q_{\alpha\beta}$ and the fluid velocity $\boldsymbol{v}$ [46–50]. In this study we employ those of Olmsted and Goldbart [47] given by

$$\rho\left(\frac{\partial}{\partial t} + \boldsymbol{v}\cdot\boldsymbol{\nabla}\right)v_{\alpha} = \partial_{\gamma}\sigma_{\gamma\alpha}, \tag{5}$$

$$N_{\alpha\beta} \equiv \left(\frac{\partial}{\partial t} + \mathbf{v}\cdot\boldsymbol{\nabla}\right)Q_{\alpha\beta} + (\kappa_{\alpha\gamma}^{[a]}Q_{\gamma\beta} - Q_{\alpha\gamma}\kappa_{\gamma\beta}^{[a]})$$

$$= \beta_1\kappa_{\alpha\beta}^{[s]} + \frac{1}{\beta_2}H_{\alpha\beta}^{[s]}, \tag{6}$$

$$\boldsymbol{\nabla}\cdot\boldsymbol{v} = 0. \tag{7}$$

Here $\kappa_{\alpha\beta} \equiv \partial_{\alpha}v_{\beta}$ is the velocity gradient tensor, ρ is the mass density of a liquid crystal assumed to be constant, and β_1 and β_2 are kinetic coefficients. The symbols $[s]$ and $[a]$ denote the symmetric and traceless part and the antisymmetric part of a second-rank tensor, respectively. We assume incompressibility of the nematic liquid crystal [Eq. (7)]. The stress tensor $\sigma_{\alpha\beta}$ is formally written as

$$\sigma_{\alpha\beta} = \sigma_{\alpha\beta}^{i[s]} + \sigma_{\alpha\beta}^{i[a]} + \sigma_{\alpha\beta}^{d} - p\delta_{\alpha\beta}, \tag{8}$$

where

$$\sigma_{\alpha\beta}^{i[s]} = \beta_3\kappa_{\alpha\beta}^{[s]} - \beta_1 H_{\alpha\beta}^{[s]}, \tag{9}$$

$$\sigma_{\alpha\beta}^{i[a]} = H_{\alpha\gamma}^{[s]}Q_{\gamma\beta} - Q_{\alpha\gamma}H_{\gamma\beta}^{[s]}, \tag{10}$$

$$\sigma_{\alpha\beta}^{d} = -\frac{\partial f\{Q_{\alpha\beta}\}}{\partial(\partial_{\alpha}Q_{\mu\nu})}\partial_{\beta}Q_{\mu\nu}. \tag{11}$$

Here $\sigma_{\alpha\beta}^{i[s]}$ is the dissipative part of the stress tensor with β_3 being a third kinetic coefficient. Note that $\beta_3/2$ is the shear viscosity also known from a conventional liquid. In Sec. III and Appendix B we will argue that due to flow-induced liquid-crystal order it is renormalized to an effective shear viscosity. The same kinetic coefficient β_1 as in Eq. (6) appears in Eq. (9), which reflects Onsager's reciprocal relation. The antisymmetric part $\sigma_{\alpha\beta}^{i[a]}$ is associated with the kinetic coupling between $Q_{\alpha\beta}$ and $\boldsymbol{v}$ arising from director rotations. $\sigma_{\alpha\beta}^{d}$ is the stress tensor due to elastic distortions. The pressure p in Eq. (8) serves as a Lagrange multiplier to ensure the incompressibility of the nematic liquid crystal [Eq. (7)].

To rescale the hydrodynamic equations, we choose the radius of the spherical particle R_0 as a unit length. We also introduce the velocity v_{∞} of the liquid crystal at infinity and set the unit time as $t_0 \equiv R_0/v_{\infty}$. We write the rescaled version of the hydrodynamic equations as

$$\mathrm{Re}\left(\frac{\partial}{\partial\bar{t}} + \bar{\boldsymbol{v}}\cdot\bar{\boldsymbol{\nabla}}\right)\bar{v}_{\alpha}$$

$$= \bar{\partial}_{\gamma}\left[2\bar{\kappa}_{\gamma\alpha}^{[s]} + \frac{1}{\mathrm{Er}^*}(-\bar{\beta}_1\bar{H}_{\gamma\alpha}^{[s]} + \bar{\sigma}_{\gamma\alpha}^{i[a]} + \bar{\sigma}_{\gamma\alpha}^{d}) - \bar{p}\delta_{\gamma\alpha}\right], \tag{12}$$

$$\bar{N}_{\alpha\beta} \equiv \left(\frac{\partial}{\partial\bar{t}} + \bar{\boldsymbol{v}}\cdot\bar{\boldsymbol{\nabla}}\right)\bar{Q}_{\alpha\beta} + (\bar{\kappa}_{\gamma\alpha}^{[a]}\bar{Q}_{\gamma\beta} - \bar{Q}_{\gamma\alpha}\bar{\kappa}_{\gamma\beta}^{[a]})$$

$$= \bar{\beta}_1\bar{\kappa}_{\alpha\beta}^{[s]} + \frac{1}{\bar{\beta}_2\mathrm{Er}^*}\bar{H}_{\alpha\beta}^{[s]}. \tag{13}$$

Here $\bar{\boldsymbol{\nabla}} = R_0\boldsymbol{\nabla}$, $\bar{\boldsymbol{v}} = v_{\infty}^{-1}\boldsymbol{v}$, and $\bar{t} = t/t_0$. We also have $\bar{\sigma}_{\alpha\beta}^{d}/\sigma_{\alpha\beta}^{d} = \bar{\sigma}_{\alpha\beta}^{i[a]}/\sigma_{\alpha\beta}^{i[a]} = 1/\Delta f$, $\bar{\kappa}_{\alpha\beta} = t_0\kappa_{\alpha\beta}$, $\bar{N}_{\alpha\beta} = (t_0/s)N_{\alpha\beta}$, and the rescaled kinetic coefficients read $\bar{\beta}_1 \equiv \beta_1/s$ and $\bar{\beta}_2 \equiv 2\beta_2 s^2/\beta_3$, where s and Δf have already been defined in connection with the rescaling of the molecular field in Eq. (3). The Reynolds number $\mathrm{Re} \equiv 2\rho v_{\infty}R_0/\beta_3$ is much smaller than unity in the present problem dealing with submicron particles. Therefore, in the following numerical calculations we set $\mathrm{Re} = 0$.

One of the important dimensionless quantities characterizing the hydrodynamic flow is the ratio of the viscous force to the elastic force of the liquid crystal

$$\mathrm{Er} = \frac{\mathrm{Er}^*}{\bar{\xi}_R^2} = \frac{\beta_3 v_{\infty}R_0}{2s^2 L_1}, \tag{14}$$

where $\bar{\xi}_R = \xi_R/R_0$. Er is nothing more than the Ericksen number [51] apart from a numerical factor.

We close this subsection by giving the relation between the kinetic coefficients in the present system and the Leslie viscosities

$$\bar{\beta}_1 = \frac{\sqrt{6}}{4}\left(-\frac{\gamma_2}{\gamma_1}\right), \quad \bar{\beta}_2 = \frac{8}{3}\frac{\gamma_1}{\alpha_4}. \tag{15}$$

The derivation of Eq. (15) is given in Appendix A. From Ref. [52], we find that the Leslie viscosities of 4-methoxbenzylidene-4′-n-butylaniline (MBBA) at $T = 44.0\,°\mathrm{C}$ (1.1 °C below the I-N transition temperature) are $\gamma_1 = -0.0228$ Pa s, $\gamma_2 = 0.0192$ Pa s, and $\alpha_4 = 0.0374$ Pa s, These values yield $\bar{\beta}_1 = 0.73$ and $\bar{\beta}_2 = 1.35$, which will be used in the following numerical calculations.

C. Setup of the system

A spherical particle of radius R_0 is fixed with its center located at the origin of the coordinate system. At infinity, a uniform flow is imposed along the z axis, so that the fluid velocity at infinity is $\boldsymbol{v} = v_{\infty}\mathbf{e}_z$, where $\mathbf{e}_z$ is the unit vector along the z direction. Since we consider the cases where the bulk liquid crystal is in an isotropic state, we set $Q_{\alpha\beta} = 0$ at infinity.

At the particle surface, the no-slip boundary condition is employed meaning $\boldsymbol{v} = \mathbf{0}$. We also impose perpendicular surface anchoring and set $\bar{Q}_{\alpha\beta} = \bar{Q}_0[e_{r\alpha}e_{r\beta} - (1/3)\delta_{\alpha\beta}]$, where $\bar{Q}_0$ is the scalar order parameter characterizing the surface-induced order and $\mathbf{e}_r$ is the unit vector along the radial direction (normal to the particle surface). We notice here that since the order parameter at the particle surface is fixed, the surface-layer phase transition as discussed in Ref. [28] is absent in the present study. We also note that from Galilei invariance, the flow and director profiles of a flowing nematic with the velocity $v_{\infty}\mathbf{e}_z$ around a fixed particle are equiva-

lent to those of a nematic at rest around a particle moving in the opposite direction with the velocity $-v_\infty \mathbf{e}_z$.

D. Calculation of the friction drag

Once a stationary profile of the orientational order parameter $Q_{\alpha\beta}$ and the fluid flow $\boldsymbol{v}$ is obtained, one can calculate the friction drag f_{fric} by

$$f_{\text{fric}} v_\infty = \int d\mathbf{r} \left[\frac{1}{\beta_2} H_{\alpha\beta}^{[s]} H_{\alpha\beta}^{[s]} + \beta_3 \kappa_{\alpha\beta}^{[s]} \kappa_{\alpha\beta}^{[s]} \right]. \quad (16)$$

Equation (16) implies that the work done by the external force f_{fric} necessary to keep the system in a stationary state is equal to the total dissipated energy in the system (right-hand side of Eq. (16). See Ref. [47]). In terms of the rescaled variables, Eq. (16) can be rewritten as

$$\frac{f_{\text{fric}}}{\beta_3 R_0 v_\infty} = \int d\bar{\mathbf{r}} \left[\frac{1}{2\bar{\beta}_2} \left(\frac{1}{\text{Er}^*} \right)^2 \bar{H}_{\alpha\beta}^{[s]} \bar{H}_{\alpha\beta}^{[s]} + \bar{\kappa}_{\alpha\beta}^{[s]} \bar{\kappa}_{\alpha\beta}^{[s]} \right], \quad (17)$$

where $\bar{\mathbf{r}} = \mathbf{r}/R_0$.

An alternative way of evaluating the force acting on the particle is to integrate the stress tensor at the particle surface. We do not adopt it because as described below, we use the vorticity instead of the pressure in determining the flow profile. An additional calculation is then necessary to evaluate the pressure at the surface. We also notice that essentially the same procedure of calculating the friction force based on the dissipation has already been employed as a numerically reliable method in Refs. [13–15].

E. Details of the numerical calculations

The numerical system is similar to that presented in our previous study [16,53,54]. In the present problem we can safely assume rotational symmetry about the z axis that is parallel to the flow direction at infinity, which renders the problem an effectively two-dimensional one. The treatment of the rotational symmetry is described in detail in Ref. [54].

We first introduce a variable $\zeta = 1 - R_0/r$, where r is the distance from the origin, the center of the particle. Then we prepare a rectangular lattice with equal grid spacings in the (ζ, θ) space, where θ is the polar angle. The number of grid points in the initial system is 33 in the ζ direction and 65 in the θ direction. Since the order parameter varies on a length scale set by the nematic coherence length $\xi_R \ll R_0$, we employ the adaptive mesh refinement procedures presented in Ref. [54]. We refine the numerical grids located in $\zeta \lesssim 0.1$ (close to the particle surface) up to two levels for $R_0/\xi_R = 200$ and one level for $R_0/\xi_R = 50$. Note that in contrast to our previous study [54], no mesh refinement/unrefinement is carried out in the course of the calculation; the numerical grids remain unchanged throughout the simulations.

We integrate Eq. (13) by a simple explicit scheme after calculating the fluid flow $\boldsymbol{v}$ at each time step. For the evaluation of $\boldsymbol{v}$, instead of directly using Eq. (12), we introduce the vorticity $\bar{\boldsymbol{\omega}} = \bar{\boldsymbol{\nabla}} \times \bar{\boldsymbol{v}}$ and eliminate the pressure $\bar{p}$ by applying the curl operator [notice that $\boldsymbol{\nabla} \times (\boldsymbol{\nabla}\bar{p}) = 0$], which, together with Re=0, yields

$$0 = \bar{\boldsymbol{\nabla}}^2 \bar{\omega}_\alpha + \frac{1}{\text{Er}^*} \epsilon_{\alpha\beta\gamma} \bar{\partial}_\beta \bar{\partial}_\delta (-\bar{\beta}_1 \bar{H}_{\delta\gamma}^{[s]} + \bar{\sigma}_{\delta\gamma}^{i[a]} + \bar{\sigma}_{\delta\gamma}^{d}), \quad (18)$$

where $\epsilon_{\alpha\beta\gamma}$ is the Levi-Civita symbol ($\epsilon_{\alpha\beta\gamma} = 1$ if α, β, γ is an even permutation of x, y, z and $\epsilon_{\alpha\beta\gamma} = -\epsilon_{\alpha\gamma\beta} = -\epsilon_{\beta\alpha\gamma}$). From the definition of $\bar{\boldsymbol{\omega}}$ and the incompressibility condition (7), we also have

$$\bar{\boldsymbol{\nabla}}^2 \bar{\boldsymbol{v}} = -\bar{\boldsymbol{\nabla}} \times \bar{\boldsymbol{\omega}}. \quad (19)$$

For a given $\bar{Q}_{\alpha\beta}$ (and therefore given $\bar{H}_{\delta\gamma}^{[s]}$, $\bar{\sigma}_{\delta\gamma}^{i[a]}$, and $\bar{\sigma}_{\delta\gamma}^{d}$), Eqs. (18) and (19) are a set of equations for $\bar{\boldsymbol{v}}$ and $\bar{\boldsymbol{\omega}}$. We use a multigrid method implemented on the numerical grid, as defined above, to solve them. Here we do not present the details of the implementation but just notice that a multigrid method is one of the efficient relaxation methods for solving partial differential equations. Interested readers may refer to Sec. 19.6 of Ref. [55] for the details of multigrid methods. The boundary conditions for $\bar{\boldsymbol{v}}$ have already been described above. For $\bar{\boldsymbol{\omega}}$, we impose $\bar{\boldsymbol{\omega}}(r=\infty) = 0$ and $\bar{\boldsymbol{\omega}}|_{r=R_0} = \bar{\boldsymbol{\nabla}} \times \bar{\boldsymbol{v}}|_{r=R_0}$ (recall the definition of $\bar{\boldsymbol{\omega}}$).

III. RESULTS AND DISCUSSIONS

We begin this section with the summary of the important dimensionless variables in the present problem; they are (i) the reduced temperature τ [see Eq. (3)], (ii) the surface order parameter $\bar{Q}_0$, (iii) the reduced particle radius $\bar{R}_0 \equiv \bar{\xi}_R^{-1} = R_0/\xi_R$ [see Eq. (4) for the definition of ξ_R], and (iv) the Ericksen number Er characterizing the fluid velocity [Eq. (14)]. We discuss the effect of these four variables in this order.

Before presenting our numerical results, we notice that

$$\tilde{\eta}_{\text{iso}} = \frac{1}{2}\beta_3 \left(1 + \frac{1}{2}\bar{\beta}_1^2 \bar{\beta}_2 \right) \quad (20)$$

should be regarded as the effective shear viscosity of an isotropic liquid crystal which replaces the bare value $1/2\beta_3$. It is valid when the fluid flow is sufficiently slow. The derivation of Eq. (20) is given in Appendix B. Here we merely mention that the correction $1/2\bar{\beta}_1^2\bar{\beta}_2$ arises from the flow-induced orientational order $\bar{Q}_{\alpha\beta}$ in the limit of small Er*. In the following we therefore plot the friction drag f_{fric} calculated by Eq. (17) in units of the Stokes friction force $6\pi\tilde{\eta}_{\text{iso}}R_0 v_\infty$ in an isotropic fluid whose shear viscosity is $\tilde{\eta}_{\text{iso}}$.

A. Effect of temperature (τ)

We plot in Fig. 1 the temperature (τ) dependence of the friction drag f_{fric} calculated by Eq. (17) for different surface order parameters ($\bar{Q}_0$). The other parameters chosen are $\bar{R}_0 = 20$ (corresponding to $R_0 \simeq 70$ nm in real units) and Er $= 0.1$ (we will give in Sec. III C a more detailed argument about the choice of Er). The temperature interval $\Delta\tau = 0.1$ corresponds to 0.90 K for 5CB [43] and 0.26 K for MBBA (material parameters given in [47] have been used). Obviously the friction drag increases with approaching the transition temperature ($\tau = 0.125$) from above. This behavior has
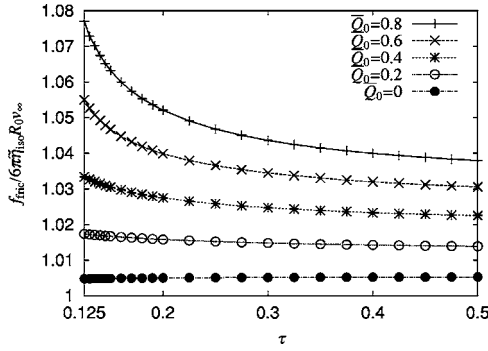
FIG. 1. Temperature (τ) dependence of the rescaled friction drag $f_{\text{fric}}/6\pi\tilde{\eta}_{\text{iso}}R_0 v_\infty$. The parameters used are $\bar{R}_0 = 20$ and Er=0.1. Note that the I-N transition temperature is $\tau = 0.125$.

FIG. 3. Surface order parameter ($\bar{Q}_0$) dependence of the rescaled friction drag $f_{\text{fric}}/6\pi\tilde{\eta}_{\text{iso}}R_0 v_\infty$. The parameters used are $\tau = 0.125$ and Er=0.1.

indeed been observed in light scattering experiments using 5CB as a host fluid [29]. Intuitively it can be understood as follows. The surface layer thickness is essentially governed by the nematic coherence length. This length decreases with increasing temperature, hence smaller layer thickness results in a smaller effect of the surface layer on the friction drag. Figure 2 plots the spatial variation of the nematic order $\text{Tr } \bar{\mathbf{Q}}^2$ around the particle. A more rapid decay of the nematic order in the case of higher temperature is clearly observed.

We also find a weaker temperature dependence of the friction drag for a smaller surface order parameter $\bar{Q}_0$. In particular, almost no effect from temperature variations is present in the case of $\bar{Q}=0$ [56]. Böttger *et al.* [29] found that the temperature dependence of the effective hydrodynamic radius (directly related to the friction drag) is weaker for smaller particle radius. They attributed it to the fact that nematic order at the surface of a smaller particle is reduced since larger elastic distortions arise from the larger surface curvature. Our findings seem to support their argument, although in Fig. 1 the particle radius is fixed and the surface order parameter is kept constant in our simulations.

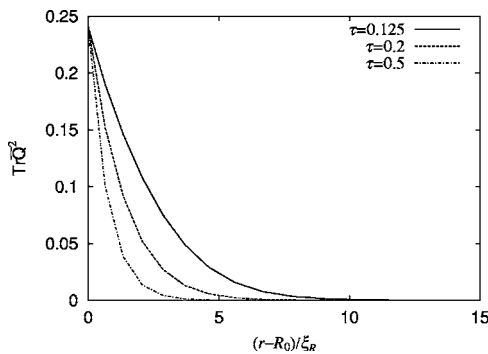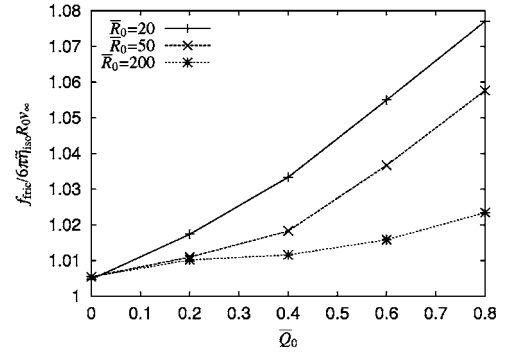One question may be raised from Fig. 1: Why do the high-temperature limits of the rescaled friction drag for different $\bar{Q}_0$'s not approach the same value? The answer is simple: The temperature is not high enough for the values of the friction drag to converge. The thickness of the surface layer, which is of the order of the nematic coherence length, must be zero for that convergence. However the coherence length approaches zero very slowly with increasing $\tau (\sim 1/\sqrt{\tau})$ and a very large τ will be necessary to achieve the convergence of the friction drag (recall that the coherence length at $\tau = 0.5$ is half as large as that at $\tau = 0.125$. See also Fig. 2). Moreover, short-coherence-length cases cannot be dealt with unless very fine numerical grids are allocated around the particle. Therefore we are not interested in the asymptotic behavior of the friction drag in the high-temperature limit.

We notice that the temperature dependence of the surface order parameter $\bar{Q}_0$ is not considered here; it is treated as a given parameter. A more realistic approach to the temperature dependence of the friction drag would take into account this temperature dependence based on the theoretical framework in Ref. [28] where a surface potential for $\bar{Q}_0$ is used. Then, the real friction drag as a function of temperature is a curve which intersects the $\bar{Q}_0$ curves in Fig. 1 at different values of τ.

FIG. 2. Variation of the nematic order ($\text{Tr } \bar{\mathbf{Q}}^2$) with the distance r from the center of the particle (in units of ξ_R) for different temperatures τ. The left-hand vertical axis corresponds to the particle surface. The data are taken along the $+z$-direction ($\theta=0$), although as shown in Fig. 6 below, the θ dependence of the orientational order is almost unobservable. The parameters used are $\bar{Q}_0=0.6$, $\bar{R}_0=20$, and Er=0.1.

B. Effect of the surface order ($\bar{Q}_0$) and the particle radius ($\bar{R}_0$)

We present in Fig. 3 how the friction drag depends on the surface order parameter $\bar{Q}_0$ for different particle radii $\bar{R}_0$. The other parameters are $\tau=0.125$ (I-N transition temperature) and Er=0.1. Figure 3 clearly indicates that the friction drag is a monotonically increasing function of $\bar{Q}_0$, which agrees with the intuition that the friction is enhanced by stronger surface order. This behavior was already visible in Fig. 1. One also finds that the effect of the surface order is more pronounced when the particle radius $\bar{R}_0$ is smaller. This can be understood intuitively from the observation that the effect of the surface nematic layer becomes less significant for larger particle radii. To rationalize our argument we show in Fig. 4 the spatial variation of the nematic order around the particle at $\tau=0.125$. In Fig. 4(a), the thickness of the surface
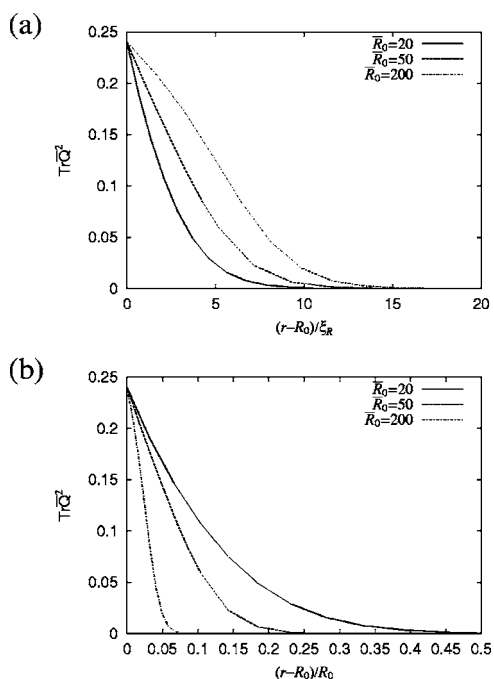
(a)

(b)

FIG. 4. Variation of the nematic order (Tr $\mathbf{Q}^2$) with the distance r from the center of the particle [in units of (a)ξ_R and (b)R_0] for different particle radii $\bar{R}_0$. As in Fig. 2, the left-hand vertical axis corresponds to the particle surface, and the data are taken along the $+z$ direction ($\theta=0$). The parameters used are $\bar{Q}_0=0.6$, $\tau=0.125$, and Er=0.1.

nematic layer itself becomes larger with increasing particle radius. In the limit of $\bar{R}_0=\infty$ (flat substrate) it diverges as $\tau \rightarrow 0.125$ [27] whereas for small particles the growth of the nematic layer is suppressed. On the other hand, Fig. 4(b) shows that when all the lengths are rescaled in units of the (unrescaled) particle radius R_0, the surface nematic order decays more rapidly for larger particle radius. So relative to the particle radius its thickness becomes less important. This behavior clearly indicates that the effect of the surface nematic layer becomes less important with increasing particle radius [57].

Figure 5 shows the effect of the reduced particle radius $\bar{R}_0$ on the rescaled friction drag. We find that the rescaled fric-
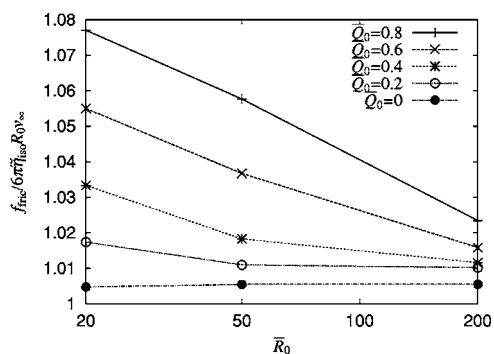

FIG. 5. Particle radius ($\bar{R}_0$) dependence of the rescaled friction drag $f_{\text{fric}}/6\pi\tilde{\eta}_{\text{iso}}R_0 v_\infty$. The parameters used are $\tau=0.125$ and Er =0.1.
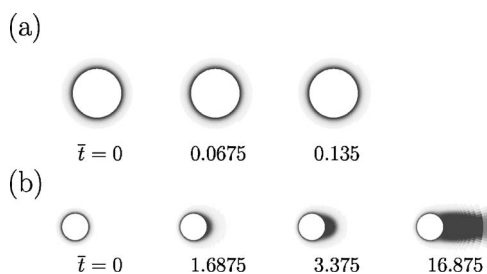
(a)

FIG. 6. Time evolution of the orientation profiles in gray-scale plots of Tr $\bar{\mathbf{Q}}^2$ for (a) Er=0.1 and (b) Er=5. In white regions the liquid crystal is in the isotropic state and it possesses nematic order in the black regions. The numbers indicate the reduced time $\bar{t}$ after the application of the flow. The other parameters are $\bar{Q}_0=0.6$, $\tau =0.125$, and $\bar{R}_0=20$. At the rightmost figures [(a)$\bar{t}=0.135$ and (b)$\bar{t} =16.875$], the system has reached a stationary state. The direction of the fluid flow is from left to right along the horizontal z axis.

tion drag decreases with increasing particle radius. As noted above, the effect of the surface nematic layer is more pronounced when the particle radius is smaller. Furthermore, the effect of the variation of the particle radius is stronger when the surface order parameter $\bar{Q}_0$ is larger.

C. Effect of the Ericksen number (Er)

Before discussing the dependence of the friction drag on the Ericksen number Er, we show in Fig. 6 the time evolution of the orientation profiles for different Ericksen numbers. The parameters used in the simulations are $\tau=0.125$, $\bar{R}_0 =20$, and $\bar{Q}_0=0.6$. For small Ericksen number (Er=0.1), we see almost no difference between the equilibrium profile, i.e., without flow ($\bar{t}=0$), and the stationary profile under flow ($\bar{t} =0.135$). This result is reasonable since an Ericksen number smaller than unity implies that the viscous force of the fluid flow is so weak that it cannot distort the orientation profile of the liquid crystal.

In contrast, for Er=5 we observe a strong effect of the fluid flow; to the right of the particle nematic order emerges ($\bar{t}=1.6875$) and evolves along the fluid flow, possibly by advection. However, the flow-induced orientational order is absent for $\bar{Q}_0<0.6$, i.e., when $\bar{Q}_0$ is smaller than the bulk order parameter at the phase transition. Furthermore, the size of the ordered region decreases considerably at slightly higher temperatures (for example, $\tau=0.130$). Therefore, the occurrence of flow-induced order in Fig. 6(b) may be attributed to the fact that at the phase transition ($\tau=0.125$) isotropic and nematic order cost the same energy so that they can coexist.

The above finding suggests that Er is not the relevant parameter to classify flow-induced order. According to its definiton [Eq. (14)], it compares viscous forces from the fluid flow to elastic forces due to director distortions around the particle of radius R_0. However, in the case presented here, orientational order first has to be created and therefore the relevant length is the nematic coherence length ξ_R. It leads to a "different" Ericksen number
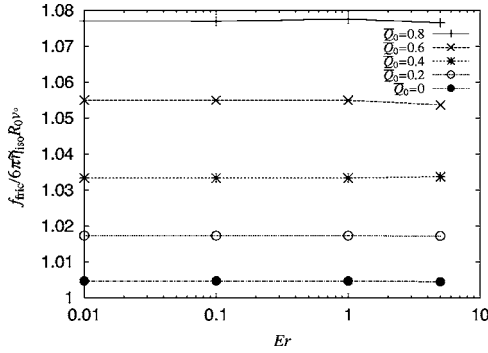
FIG. 7. Ericksen number (Er) dependence of the rescaled friction drag $f_{\rm fric}/6\pi\tilde{\eta}_{\rm iso}R_0 v_\infty$. The parameters used are $\tau=0.125$ and $\bar{R}_0=20$.

$$\widetilde{\rm Er} \equiv \frac{\beta_3 v_\infty \xi_R}{2s^2 L_1} = \frac{\rm Er}{\bar{R}_0}, \tag{21}$$

which for the present case (Er=5 and $\bar{R}_0=20$) gives $\widetilde{\rm Er}=0.25$, i.e., a value smaller than one. Therefore, except for the special case of $\tau=0.125$ and $\bar{Q}_0\gtrsim0.6$, we do not expect a pronounced flow-induced order. Indeed, in some preliminary calculations with $\widetilde{\rm Er}=1$ (Er=20) flow-induced order is clearly observed for wide ranges of $\bar{Q}_0$ and τ, even in the case of $\bar{Q}_0=0$ and $\tau=0.150$ [58].

Figure 7 plots the dependence of the friction drag $f_{\rm fric}$ on the Ericksen number. The rescaled friction drag $f_{\rm fric}/6\pi\tilde{\eta}_{\rm iso}R_0 v_\infty$ is essentially independent of Er, although it exhibits a very slight decrease for Er=5 and $\bar{Q}_0=0.6$ or 0.8. We have already stated that for $Q_0<0.6$ the equilibrium profile of the order parameter is hardly affected for flow fields with Er up to five. So it is clear that the friction drag is constant. On the other hand, it is somewhat surprising that even in the presence of flow-induced order (Er=5, $\bar{Q}_0=0.6$ or 0.8), the rescaled friction drag shows almost no dependence on Er. We have no clear understanding for this observation and expect that at higher Ericksen numbers the friction drag will be altered. As noted in [58], however, at present we cannot deal with large Er cases in a quantitative manner.

We also note that for small particles it is quite difficult to achieve large Er. When we choose typical values for the material parameters, $\beta_3=4\times10^{-2}$ Pa s and $\Delta f=L_1 s^2/\xi_R^2=3\times10^5$ J m^{-3}, we find from Eq. (14) that v_∞ must be as large as 1.5 cm/s to realize Er=5 in the case of $\bar{R}_0=20(R_0\simeq70$ nm). Therefore except for extremely large Ericksen numbers that do not seem to be accessible experimentally, we can regard the rescaled friction drag as independent of Er. In most of the calculations shown in the previous subsections, we therefore have chosen Er=0.1, in which case no flow-induced order occurs.

IV. CONCLUDING REMARKS

We investigated the friction drag of a spherical particle in a liquid crystal above the isotropic-nematic transition by solving the hydrodynamic equations for the fluid velocity and the orientational order parameter represented by a second-rank tensor. We were interested in the effect of the surface nematic layer induced at the particle surface, which was taken into account in our numerical calculations by fixing the orientational order parameter at the surface. Rigid normal anchoring was imposed at the particle surface and produced a director field pointing along the radial direction in the absence of external flow.

All parameters in the system can be represented by four dimensionless variables: the reduced temperature τ, the surface order parameter $\bar{Q}_0$; the particle radius $\bar{R}_0$ in units of the nematic coherence length; and the Ericksen number Er. We showed that the friction drag increases when the isotropic-nematic phase transition is approached from above and that the effect of temperature variations is stronger when the system is closer to the transition. This result reproduces previous experiments measuring the effective hydrodynamic radius of a suspended particle in a liquid crystal. We also found that a larger surface order parameter yields a stronger temperature dependence of the friction drag.

The variation of the surface order parameter has a pronounced effect on the friction drag; it increases monotonically with the surface order parameter. We also showed that the effect of the surface nematic layer is more pronounced in the case of smaller particles. These results are in agreement with intuition.

From the observation of the profiles of the orientational order, we found that just above the transition point the fluid flow can induce orientational order away from the particle, possibly by advection, when the Ericksen number is large (Er=5) and the surface order is sufficiently strong ($\bar{Q}_0\gtrsim0.6$). Nevertheless, the rescaled friction drag is almost independent of Er for Er≤5.

We comment on a direct quantitative comparison of our numerical results with possible experiments. In our numerical calculations, the order parameter at the particle surface was fixed, so its temperature dependence was not taken into account. Such a temperature dependence can, however, be calculated within the theoretical framework of our previous work [28] where we introduced a surface free energy for the orientational order parameter and a proper method to treat wetting transitions. Such a calculation would finally give a more direct comparison of the numerical data to experiments. Nevertheless, the numerical work presented in this paper gives a clear account of the main features in the dynamical behavior of liquid crystal colloids close to the isotropic-nematic phase transition.

Finally, we discuss the possibility of an experimental observation of the flow-induced orientational order. An indirect way of detecting the flow-induced order would be a viscosity measurement of colloidal dispersions with liquid crystal hosts. In the absence of flow-induced order, it is expected that a dilute colloidal dispersion behaves as a Newtonian fluid whose viscosity obeys the Einstein formula $\eta_{\rm eff}/\eta=1+5/2\phi$ (where the volume fraction ϕ should be renormalized because of nematic wetting layers at the particle surfaces). However, flow-induced order around particles under a very strong flow would lead to non-Newtonian behavior of the

dispersion. A change in the shear viscosity would therefore indicate the occurrence of flow-induced order around particles.

More direct evidence of flow-induced order would be obtained by optical observation of birefringence due to induced orientational order. Optical tweezers have been successfully and extensively used to manipulate colloidal particles in liquid crystal hosts [25,60], and in the present case they will provide a promising way to move a particle so fast as to attain large Ericksen numbers (alternatively, they can be used to fix a particle in a flowing liquid crystal). As proposed in [15], a falling-ball experiment using micron-sized gold particles will be another possible candidate for the experimental observation of the flow-induced order, because large particles would allow one to achieve large Ericksen numbers (Er $\propto R_0^3$ and $\widetilde{\mathrm{Er}} \propto R_0^2$, the terminal velocity is proportional to R_0^2) and large mass density difference between the gold particle and the liquid crystal is also preferable. Moreover, a different geometry can be considered: a particle fixed between two flat parallel substrates constituting a liquid crystal cell. In this case the fluid velocity can be chosen large so that high Ericksen numbers are achieved more easily. Although this geometry is different from the one in our study, it is considered as an experimentally accessible system that allows the observation of flow-induced nematic order around a particle. The flow property around an obstacle in a liquid crystal cell is one of the important subjects of the liquid crystal industry and we hope that experimental studies along this direction will be promoted by our work.

ACKNOWLEDGMENTS

APPENDIX A: DERIVATION OF THE RELATION BETWEEN $\bar{\beta}_{1,2}$ AND THE LESLIE VISCOSITIES

Substituting the uniaxial form of the order parameter $Q_{\alpha\beta} = Q_0(n_\alpha n_\beta - (1/3)\delta_{\alpha\beta})$ into Eq. (6), one obtains

$$N_\alpha \equiv \left(\frac{\partial}{\partial t} + \boldsymbol{v}\cdot\boldsymbol{\nabla} + \kappa_{\alpha\gamma}^{[a]}n_\gamma\right) = \frac{1}{Q_0}\left(\beta_1 \kappa_{\alpha\beta}^{[s]}n_\beta + \frac{1}{\beta_2}H_{\alpha\beta}^{[s]}n_\beta\right).$$

(A1)

We note that in Eq. (A1), only the components perpendicular to **n** are relevant [7] and those parallel to **n** have been dropped. Comparing Eq. (A1) with the Ericksen-Leslie equation [7] $h_\alpha = \gamma_1 N_\alpha + \gamma_2 \kappa_{\alpha\beta}^{[s]}n_\beta$ (h_α is the molecular field in terms of **n**), we have

$$\beta_1 = Q_0\left(-\frac{\gamma_2}{\gamma_1}\right).$$

(A2)

Under the one-constant approximation, the elastic energy density in terms of **n** is $f = (K/2)(\partial_\alpha n_\beta)^2$, where K is the Frank elastic constant. Again by substituting $Q_{\alpha\beta} = Q_0(n_\alpha n_\beta - (1/3)\delta_{\alpha\beta})$ into Eq. (1), we find that $K = 2L_1 Q_0^2$. Since the molecular field in terms of **n** is $h_\alpha = K\nabla^2 n_\alpha$, one has $H_{\alpha\beta}^{[s]}n_\beta = (1/2Q_0)h_\alpha$. Then from Eq. (A1) and the Ericksen-Leslie equation

$$\beta_2 = \frac{\gamma_1}{2Q_0^2}.$$

(A3)

At the isotropic-nematic transition point, $Q_0 = (\sqrt{6}/4)s$ (see Sec. II A). Recalling the definition of rescaled kinetic coefficients $\bar{\beta}_1$ and $\bar{\beta}_2$ given after Eq. (13), we finally arrive at Eq. (15) from Eqs. (A2) and (A3). Here we have used the relation $\beta_3 = \alpha_4$, deduced from a direct comparison of Eq. (9) with the stress tensor of the Ericksen-Leslie equation.

APPENDIX B: SHEAR VISCOSITY OF AN ISOTROPIC LIQUID CRYSTAL η_{iso}

In this appendix we show that the bare shear viscosity $1/2\beta_3$ of an isotropic liquid crystal is renormalized by flow-induced order. One has to take into account the contribution of the molecular field $H_{\alpha\beta}$, because the contribution from the flow-induced orientational order $\bar{Q}_{\alpha\beta}$ is not at all negligible even when the flow-induced order is very small in a weak flow. In fact, in the cases where $Q_{\alpha\beta} \simeq 0$, the molecular field behaves as $\bar{H}_{\alpha\beta}^{[s]} = -\bar{\beta}_1\bar{\beta}_2\mathrm{Er}^*\bar{\kappa}_{\alpha\beta}^{[s]} + O[(\mathrm{Er}^*)^2]$ for small Ericksen numbers [see Eq. (13)]. Since the rescaled velocity gradient tensor $\bar{\kappa}_{\alpha\beta}^{[s]}$ is of order unity, it can be shown from Eq. (3) that $\bar{Q}_{\alpha\beta} = O(\mathrm{Er}^*)$, which is *a posteriori* consistent with Eq. (13). In the case of $\bar{Q}_0 = 0$ at the particle surface (corresponding to a disordering surface; contribution of the surface order is absent), $\bar{Q}_{\alpha\beta} = O(\mathrm{Er}^*)$ should be satisfied throughout the system in the case of weak flow $\mathrm{Er}^* \ll 1$. Then from Eq. (17), we find

$$\frac{f_{\mathrm{fric}}}{6\pi R_0 v_\infty} \simeq \frac{1}{2}\beta_3\left(1 + \frac{1}{2}\bar{\beta}_1^2\bar{\beta}_2\right)\int d\bar{r}\frac{1}{3\pi}\bar{\kappa}_{\alpha\beta}^{[s]}\bar{\kappa}_{\alpha\beta}^{[s]}.$$

(B1)

In the case of Stokes flow, $\int d\bar{r}(1/3\pi)\bar{\kappa}_{\alpha\beta}^{[s]}\bar{\kappa}_{\alpha\beta}^{[s]} = 1$. Hence if the deviation of the flow profile from the Stokes one is small enough, we finally obtain

$$\frac{f_{\mathrm{fric}}}{6\pi R_0 v_\infty} \simeq \frac{1}{2}\beta_3\left(1 + \frac{1}{2}\bar{\beta}_1^2\bar{\beta}_2\right).$$

(B2)

The right-hand-side of Eq. (B2) defines $\widetilde{\eta}_{\mathrm{iso}}$, Eq. (20). The numerical results presented in Fig. 3 indeed demonstrates that in the case of $\bar{Q}_0 = 0$ and $\tau = 0.125$, $f_{\mathrm{fric}}/6\pi R_0 v_\infty = 1.005 \times \widetilde{\eta}_{\mathrm{iso}} (= 1.366 \times 1/2 \beta_3)$ irrespective of the particle size. The agreement of the numerically obtained viscosity $f_{\mathrm{fric}}/6\pi R_0 v_\infty$ with $\widetilde{\eta}_{\mathrm{iso}}$ indicates that $\widetilde{\eta}_{\mathrm{iso}}$ rather than $1/2 \beta_3$ should be regarded as the effective shear viscosity of an isotropic liquid crystal.

We note also that from Eqs. (6) and (9) one obtains

$$\sigma_{\alpha\beta}^{i[s]} = \beta_3\left(1 + \frac{1}{2}\bar{\beta}_1^2\bar{\beta}_2\right)\kappa_{\alpha\beta}^{[s]} - \beta_1\beta_2 N_{\alpha\beta}. \qquad (B3)$$

This formulation of the dissipative stress $\sigma_{\alpha\beta}^{i[s]}$ in terms of the time variation of the order parameter $N_{\alpha\beta}$ is in complete parallel with the Ericksen-Leslie equations of a nematic liquid crystal [7] and has indeed been employed by Qian and Sheng [48] in the derivation of the hydrodynamic equation of $Q_{\alpha\beta}$. In the case of an isotropic liquid crystal, $Q_{\alpha\beta}=O(\mathrm{Er}^*)$

leads to $N_{\alpha\beta}=O(\mathrm{Er}^*)$, that is, the contribution of the second term in the right-hand side of Eq. (B3) is negligible compared to the first one. Therefore Eq. (B3) again yields the conclusion that $\tilde{\eta}_{\mathrm{iso}}=1/2\ \beta_3(1+1/2\ \bar{\beta}_1^2\bar{\beta}_2)$ has to be considered as the effective shear viscosity of the isotropic liquid crystal. It may be worthwhile to notice that Ref. [59] gives similar arguments about the interpretation of the effective viscosity measured in ultrasonic sound attenuation experiments.

[1] W. B. Russel, D. A. Saville, and W. R. Schowalter, *Colloidal Dispersions* (Cambridge University Press, Cambridge, England, 1989).

[2] L. D. Landau and E. M. Lifshitz, *Fluid Mechanics* (Pergamon Press, Oxford, 1959).

[3] G. G. Stokes, Trans. Cambridge Philos. Soc. **9**, 8 (1851).

[4] A. Einstein, Ann. Phys. **17**, 549 (1905).

[5] A. Einstein, Ann. Phys. **19**, 289 (1906); **34**, 591 (1911).

[6] A. Einstein, Ann. Phys. **19**, 371 (1906).

[7] P. G. de Gennes and J. Prost, *The Physics of Liquid Crystals*, 2nd ed. (Oxford University Press, New York, 1993).

[8] S. Chandrasekhar, *Liquid Crystals*, 2nd ed. (Cambridge University Press, Cambridge, England, 1992).

[9] A. C. Diogo, Mol. Cryst. Liq. Cryst. **100**, 153 (1983).

[10] V. G. Roman and E. M. Terentjev, Colloid J. USSR **51**, 435 (1989) [Kolloidn. Zh. **51**, 507 (1989)].

[11] H. Kneppe, F. Schneider, and B. Schwesinger, Mol. Cryst. Liq. Cryst. **205**, 9 (1991).

[12] H. Heuer, H. Kneppe, and F. Schneider, Mol. Cryst. Liq. Cryst. Sci. Technol., Sect. A **214**, 43 (1992).

[13] R. W. Ruhwandl and E. M. Terentjev, Phys. Rev. E **54**, 5204 (1996).

[14] H. Stark and D. Ventzki, Phys. Rev. E **64**, 031711 (2001).

[15] H. Stark and D. Ventzki, Europhys. Lett. **57**, 60 (2002); H. Stark, D. Ventzki, and M. Reichert, J. Phys.: Condens. Matter **15**, S191 (2003).

[16] J. Fukuda, H. Stark, M. Yoneya and H. Yokoyama, *20th International Liquid Crystal Conference*, Slovenia, 2004; (International Liquid Crystal Society, USA, 2004); Mol. Cryst. Liq. Cryst. Sci. Technol., Sect. A (to be published).

[17] H. Heuer, H. Kneppe, and F. Schneider, Mol. Cryst. Liq. Cryst. **200**, 51 (1991).

[18] R. W. Ruhwandl, and E. M. Terentjev, Z. Naturforsch. A **50A**, 1023 (1995).

[19] S. Chono and T. Tsuji, Mol. Cryst. Liq. Cryst. Sci. Technol., Sect. A **309**, 217 (1998).

[20] A. E. White, P. E. Cladis, and S. Torza, Mol. Cryst. Liq. Cryst. **43**, 13 (1977).

[21] E. Kuss, Mol. Cryst. Liq. Cryst. **47**, 71 (1978).

[22] Z. Sun, J. Fang, N. Ming, and X. Tang, Phys. Lett. A **14**, 284 (1990).

[23] V. G. Bhide, and M. C. Kandpal, Phys. Rev. B **20**, 85 (1979).

[24] H. M. Widatallah, Y. F. Hsia, N. Fang, and X. M. Lee, Phys. Lett. A **215**, 326 (1996); Y. F. Hsia, N. Fang, H. M. Widatallah, D. M. Wu, X. M. Lee, and J. R. Zhang, Hyperfine Interact. **126**, 401 (2000).

[25] T. A. Wood, *20th International Liquid Crystal Conference*, Slovenia, 2004. (International Liquid Crystal Society, USA, 2004).

[26] J. C. Loudet, P. Hanusse, and P. Poulin, Science **306**, 1525 (2004).

[27] P. Sheng, Phys. Rev. A **26**, 1610 (1982).

[28] J. Fukuda, H. Stark, and H. Yokoyama, Phys. Rev. E **69**, 021714 (2004); H. Stark, J. Fukuda, and H. Yokoyama, J. Phys.: Condens. Matter **16**, S1911 (2004).

[29] A. Böttger, D. Frenkel, E. van de Riet, and R. Zijlstra, Liq. Cryst. **2**, 539 (1987)

[30] P. G. de Gennes, Mol. Cryst. Liq. Cryst. **12**, 193 (1971).

[31] D. J. Cleaver and P. Ziherl. eds., *Proceedings of an ESF PESC Exploratory Workshop on Liquid Crystal Colloid Dispersions* (J. Phys.: Condens. Matter Vol. **16**, Number 19).

[32] P. Poulin, V. A. Raghunathan, P. Richetti, and D. Roux, J. Phys. II **4**, 1557 (1994); V. A. Raghunathan, P. Richetti, and D. Roux, Langmuir **12**, 3789 (1996); V. A. Raghunathan, P. Richetti, D. Roux, F. Nallet, and A. K. Sood, Mol. Cryst. Liq. Cryst. Sci. Technol., Sect. A **288**, 181 (1996); Langmuir **16**, 4720 (2000).

[33] P. Poulin, H. Stark, T. C. Lubensky, and D. A. Weitz, Science **275**, 1770 (1997); P. Poulin and D. A. Weitz, Phys. Rev. E **57**, 626 (1998); J.-C. Loudet, P. Barois, and P. Poulin, Nature (London) **407**, 611 (2000); J. C. Loudet, P. Poulin, and P. Barois, Europhys. Lett. **54**, 175 (2001); J. C. Loudet, P. Barois, P. Auroy, P. Keller, H. Richard, and P. Poulin, Langmuir **20**, 11336 (2004).

[34] M. Zapotocky, L. Ramos, P. Poulin, T. C. Lubensky, and D. A. Weitz, Science **283**, 209 (1999); L. Ramos, M. Zapotocky, T. C. Lubensky, and D. A. Weitz, Phys. Rev. E **66**, 031711 (2002).

[35] J. Yamamoto and H. Tanaka, Nature (London) **409**, 321 (2001).

[36] V. G. Nazarenko, A. B. Nych, and B. I. Lev, Phys. Rev. Lett. **87**, 075504 (2001); I. I. Smalyukh, S. Cherryshuk, B. I. Lev, A. B. Nych, U. Ognysta, V. G. Nazarenko, O. D. Lavrentovic *ibid.* **93**, 117801 (2004).

[37] M. Mitov, C. Portet, C. Bourgerette, E. Snoeck, and M. Verelst, Nat. Mater. **1**, 229 (2002); M. Mitov, C. Bourgerette, and F. de Guerville, J. Phys.: Condens. Matter **19**, S1981 (2004).

[38] T. Bellini, M. Caggioni, N. A. Clark, F. Mantegazza, A. Maritan, and A. Pelizzola, Phys. Rev. Lett. **91**, 085704 (2003).

[39] S. P. Meeker, W. C. K. Poon, J. Crain, and E. M. Terentjev, Phys. Rev. E **61**, R6083 (2000); V. J. Anderson, E. M. Terentjev, S. P. Meeker, J. Crain, and W. C. K. Poon, Eur. Phys. J.

E **4**, 11 (2001); V. J. Anderson and E. M. Terentjev, *ibid.* **4**, 21 (2001); D. Vollmer, G. Hinze, W. C. K. Poon, J. Cleaver, and M. E. Cates, J. Phys.: Condens. Matter **16**, L227 (2004); J. Cleaver and W. C. K. Poon, *ibid.* **16**, S1901 (2004).

[40] J. L. West, A. Glushchenko, G. Liao, Y. Reznikov, D. Andrienko, and M. P. Allen, Phys. Rev. E **66**, 012702 (2002).

[41] A. Borštnik, H. Stark, and S. Žumer, Phys. Rev. E **60**, 4210 (1999); **61**, 2831 (2000).

[42] P. Galatola and J.-B. Fournier, Phys. Rev. Lett. **86**, 3915 (2001); J.-B. Fournier and P. Galatola, Phys. Rev. E **65**, 032702 (2002); H. Stark, *ibid.* **66**, 041705 (2002); P. Galatola, J.-B. Fournier, and H. Stark, *ibid.* **67**, 031404 (2003).

[43] H. Stark, J. Fukuda, and H. Yokoyama, Phys. Rev. Lett. **92**, 205502 (2004).

[44] D. Andrienko, P. Patrício, and O. I. Vinogradova, J. Chem. Phys. **121**, 4414 (2004).

[45] M. Huber and H. Stark, Europhys. Lett. **69**, 135 (2005).

[46] S. Hess, Z. Naturforsch. A **30A**, 728 (1975).

[47] P. D. Olmsted and P. Goldbart, Phys. Rev. A **41**, R4578 (1990); **46**, 4966 (1992).

[48] T. Qian and P. Sheng, Phys. Rev. E **58**, 7475 (1998).

[49] H. Pleiner, M. Liu, and H. R. Brand, Rheol. Acta **41**, 375 (2002).

[50] H. Stark and T. C. Lubensky, Phys. Rev. E **67**, 061709 (2003).

[51] P. G. de Gennes, in *Molecular Fluids*, edited by R. Balian and G. Weill (Gordon and Breach, London, 1976), pp. 373–400.

[52] H. Kneppe, F. Schneider, and N. K. Sharma, J. Chem. Phys. **77**, 3203 (1982).

[53] J. Fukuda, M. Yoneya, and H. Yokoyama, Phys. Rev. E **65**, 041709 (2002); Mol. Cryst. Liq. Cryst. **413**, 221 (2004); J. Fukuda, H. Stark, M. Yoneya, and H. Yokoyama, J. Phys.: Condens. Matter **16**, S1957 (2004);

[54] J. Fukuda, M. Yoneya, and H. Yokoyama, Eur. Phys. J. E **13**, 87 (2004).

[55] W. H. Press, S. A. Teukolsky, W. T. Vetterling, and B. P. Flannery, *Numerical Recipes in C*, 2nd ed. (Cambridge University Press, Cambridge, 1992).

[56] This result may look strange and counterintuitive. But notice that in the argument of Appendix B, temperature does not appear explicitly. Therefore the temperature dependence of the friction drag may well be absent; it would arise from the variation of the kinetic coefficients with temperature, which is not taken into account in our calculation.

[57] Another rough argument supports the discussion here; the surface layer thickness behaves as $\ln R_0$, and the effect of surface nematic order becomes less important for a larger particle because $\ln R_0 / R_0 \rightarrow 0$ as $R_0 \rightarrow \infty$. The wetting layer thickness in critical binary fluids is shown to diverge as the minus of the logarithm of the undersaturation [J. W. Cahn, J. Chem. Phys. **66**, 3667 (1977)]. In our case the effective temperature raise due to curvature, which is of the order of R_0^{-1} [28], corresponds to the undersaturation.

[58] We do not present results for $\widetilde{\mathrm{Er}}=1$ (Er=20) because it is quite difficult to obtain numerically reliable stationary profiles under a strong flow; the region with flow-induced order extends far away from the particle so that very high numerical resolutions are necessary in this region as well as close to the particle. So heavy calculations are required. For this reason, we have to restrict ourselves to the cases with $Er \leqslant 5$ in the present paper.

[59] Reference [7], Sec. 5.2.2. It is the molecular field that is considered to be negligible there and the viscous coefficients ν_i's in the Harvard notation are equal to the measured viscosities. On the other hand, they are nontrivial functions of Leslie viscosities.

[60] Y. Iwashita and H. Tanaka, Phys. Rev. Lett. **90**, 045501 (2003); M. Yada, J. Yamamoto, and H. Yokoyama, *ibid.* **92**, 185501 (2004); I. Muševič, M. Skarabot, D. Babic, N. Osterman, I. Poberaj, V. Nazarenko, and A. Nych, *ibid.* **93**, 187801 (2004); I. I. Smalyukh *et al.*, Appl. Phys. Lett. **86**, 021913 (2005).